

LES and RANS of turbulent flow in tube bundles

P. Rollet-Miet^{a,b}, D. Laurence^{a,b,*}, J. Ferziger^c

^a EDF-DER-LNH, 6 quai Watier, 78401 Chatou, France

^b LMFA UMR CNRS 5509, Ecole Centrale de Lyon, 69131 Ecully, France

^c Department of Civil Engineering, Stanford University, Stanford, CA 94309-4020, USA

Abstract

A Large Eddy Simulation (LES) finite element code is developed. It is shown that the standard numerical schemes developed for the Reynolds Averaged Navier–Stokes (RANS) equations are not suitable for LES. Validation of the final centred and collocated scheme is carried out for grid turbulence and channel flow. The same code is then applied to a complex flow that has challenged RANS modelling for years: cross-flow in a tube bundle. In contrast to RANS models, LES yields results in good agreement with the experimental data of Simonin and Barouda (1988, Measurements and prediction of turbulent flow entering a staggered tube bundle. Fourth International Symposium on Applications of Laser Anemometry to Fluid Mechanics, Lisbon, Portugal) including the Reynolds stresses. © 1999 Elsevier Science Inc. All rights reserved.

1. Introduction

Large Eddy Simulation (LES) has long been restricted to simple building block flows (homogeneous or channel flows), while models for Reynolds Averaged Navier–Stokes (RANS) equations are commonly applied to three-dimensional flows in complex geometries. Some fairly complex domains have been simulated by LES: flow around a cube and a square cylinder (Rodi et al., 1997). However LES requires severe mesh refinement near the body, and with structured meshes a very large number of mesh points are required. The advantage of unstructured grids is the admission of local mesh refinement (Jansen, 1993). On the other hand, the highly accurate schemes used for LES (pseudo-spectral or Padé schemes) are applicable only to cartesian grids. Only two applications of LES codes on unstructured grids for incompressible flow have been made (Jansen, 1993; Ducros et al., 1997). We present here the development of an LES code for incompressible fluid based on a finite element method (Rollet-Miet, 1997). This LES version is based on the N3S code developed by Chabard and Métivet (1992).

The organisation of this paper is as follows. Numerical issues are explored in Section 2. The effect of numerical method on LES of channel flow is analysed in Section 3. The final numerical method is applied to tube bundle flow in Section 4. This flow is of particular interest to the power generation industry, where not only the performance of heat exchangers needs to be studied, but also risks of vibrations induced by fluid–structure coupling and large scale temperature fluctuations inducing thermal stresses, both factor which can lead to premature ageing of this component of a power plant. Fortunately for LES, this is also one of the rare industrial flows

where periodic boundary conditions are not apt to be questioned.

2. Numerical issues

In contrast to the RANS method, with LES one explicitly computes the large scales of motion and introduces a model only for the small motions. LES is based upon the application of a spatial filtering operation (denoted by a bar) to the three-dimensional unsteady Navier–Stokes equations. We assume, and subsequently check from energy spectra, that the filtering allows the flow to be captured on the computational grid.

Let \bar{u} be the (filtered) velocity of large scale motion. The subgrid-scale stresses (SGS) τ_{ij} result from the influence of unresolved scales on large scales, and are defined by $\tau_{ij} = \bar{u}_i \bar{u}_j - \bar{u}_i \bar{u}_j$.

The filtered Navier–Stokes and continuity equations are:

$$\frac{\partial \bar{u}_i}{\partial t} + \frac{\partial \bar{u}_i \bar{u}_j}{\partial x_j} = -\frac{1}{\rho} \frac{\partial \bar{p}}{\partial x_i} + \nu \frac{\partial^2 \bar{u}_i}{\partial x_j \partial x_j} - \frac{\partial \tau_{ij}}{\partial x_j}, \quad \frac{\partial \bar{u}_i}{\partial x_i} = 0.$$

The Smagorinsky model is a simple mixing length model for the deviator of the subgrid-stresses:

$$\tau_{ij}^d = \tau_{ij} - \frac{1}{3} \tau_{kk} \delta_{ij} = -2\nu_t \bar{S}_{ij} = -2C\bar{\Delta}^2 |\bar{S}| \bar{S}_{ij}$$

with ν_t the turbulent viscosity, $\bar{\Delta}$ the characteristic length scale ($\bar{\Delta} = 2h$), and with h the mesh spacing for a regular mesh. \bar{S}_{ij} is the filtered strain rate tensor:

$$\bar{S}_{ij} = \frac{1}{2} \left(\frac{\partial \bar{u}_i}{\partial x_j} + \frac{\partial \bar{u}_j}{\partial x_i} \right) \quad \text{and} \quad |\bar{S}| = (2\bar{S}_{ij} \bar{S}_{ij})^{1/2}$$

$C = C_S^2$, C_S is the Smagorinsky constant.

* Corresponding author. E-mail: dominique.laurence@der.edf.fr.

Subgrid-modelling is an important problem for LES, but we focus on the requirements of numerical schemes for LES on unstructured grids.

2.1. Time advancement

Two different methods have been tested: the method of characteristics, and the centred Adams–Bashforth, Crank–Nicholson scheme (AB–CN).

The characteristics scheme deals only with the advection step and is used within a fractional time-step method. For pure advection, velocities are conserved along the characteristic curve defined by: $dx/dt = u$; $dy/dt = v$; $dz/dt = w$. At each time step t^n , this curve is followed backwards from each node. Once the location of the fluid particle at t^{n-1} is known, the velocity is interpolated by quadratic or higher-order interpolation functions. Then the Stokes problem will be solved for this intermediate velocity field.

This approach is very attractive, because it introduces a natural upwinding and is unconditionally stable: it is used frequently for the $k-\epsilon$ calculations. For steady state problems, it has very low numerical diffusion since cubic or Hermitian interpolation can be used. But, for the highly unsteady flow in LES, since the discretized characteristics method uses interpolation in both space and time, the first-order temporal interpolation results in unacceptable numerical damping. As for any upwind scheme, the artificial viscosity can be computed. In 1D, on a regular grid with advection velocity u

$$\frac{\partial f(t, x)}{\partial t} \approx \frac{f(t^{n+1}, x) - f(t^n, x)}{\Delta t} = \frac{f(t^n, x - u \Delta t) - f(t^n, x)}{\Delta t}$$

Introducing a Taylor expansion of $f(t^n, x - u \Delta t)$ yields

$$\frac{\partial f}{\partial t} \approx -u \frac{\partial f}{\partial x} + v_{\text{num}} \frac{\partial^2 f}{\partial x^2} + o(\Delta x, \Delta t)$$

with $v_{\text{num}} = \frac{1}{2} u^2 \Delta t = \frac{1}{2} u c \Delta x$, where c is the Courant number.

The scheme is first-order accurate in time or equivalently in space, whatever the order of the spatial interpolation at the end of the characteristic. This problem was identified in (Laurence, 1985) and resolved for cartesian grids by introducing a moving frame of reference at each time step, but cannot be extended to unstructured grids.

The classical AB–CN scheme was chosen to evaluate the benefits of a centred scheme. In the variational formulation it gives

$$\begin{aligned} & \int_{\Omega} \frac{\bar{\mathbf{u}} - \bar{\mathbf{u}}^n}{\Delta t} \mathbf{v} \, d\Omega + \frac{1}{2} \int_{\Omega} (v_i + v_i) \nabla \bar{\mathbf{u}} \cdot \nabla \mathbf{v} \, d\Omega \\ &= - \int_{\Omega} \bar{p}^n \nabla \mathbf{v} \, d\Omega - \frac{1}{2} \int_{\Omega} (v_i + v_i) \nabla \bar{\mathbf{u}}^n \cdot \nabla \mathbf{v} \, d\Omega \\ & \quad - \frac{3}{2} C^n + \frac{1}{2} C^{n-1} + \text{boundary terms} \end{aligned}$$

with $\bar{\mathbf{u}}$ the velocity field after the advection–diffusion step and \mathbf{v} the weighting function.

The influence of the formulation of convective term has been investigated in detail, but not in the FEM context (Horiuti, 1987; Laurence, 1985). Here we chose the straightforward advective formulation:

$$C_i^n = \int_{\Omega} u_k^n \frac{\partial u_i^n}{\partial x_k} \mathbf{v} \, d\Omega.$$

Linear basis functions are used in the variational formulation: the scheme is fourth-order accurate for the convective term and second-order for the diffusive term (Bercovier and Pironneau, 1977). However, to avoid the computational cost

of inverting the mass-matrix, this matrix is condensed on the diagonal, providing a second-order accurate scheme. Linear analysis shows that this scheme is stable for a Courant number less than 0.2.

These schemes were compared for isotropic turbulence decay. Comparison of the energy spectra with experiments do not tell much since the dynamic model automatically decreases the Smagorinsky constant if a dissipative scheme is used (this is hardly acceptable for other than grid turbulence). The spectral transfer is more significant. The change of the spectrum of the turbulent kinetic energy during the advection step was evaluated for 50 samples. The averaged variation is drawn in Fig. 1 for two meshes: a coarse one ($N = 32$ points on a domain edge) and a refined one ($N = 64$ points). Spectral analysis shows that, for homogeneous turbulent flow, the advection term produces a transfer of energy from the larger structures (small wave number k) to the smaller ones (large k). The numerical test shows that the characteristic scheme is dissipative on average and very dependent of the grid: due to the highly unsteady nature of the smaller scales, the first-order accurate nature of the scheme is unacceptable. On the contrary, the centred scheme effectively transfers energy from the small wave numbers to the large ones and is relatively independent of the spatial resolution.

We stress here that the paradoxical choices of upwind biased schemes for most RANS computations and centred schemes for LES should be analysed in the spatial–temporal frame, and is due to the highly unsteady nature of the smallest resolved scales in LES.

2.2. Spatial discretization

The spatial discretization relies on tetrahedral elements, permitting great flexibility in meshing. We restricted ourselves to linear shape functions. We introduce the P1–P1 element based on collocated velocity and pressure nodes (Fig. 2) (hardly ever used in the F.E. literature, except to point out its defects). The standard finite element discretization (used in the N3S code) is the P1–isoP2 element (Fig. 2) based on two levels of discretization: the pressure is interpolated linearly on the macro-element, while the velocity is interpolated linearly on each subelement.

The P1–isoP2 element satisfies the well-known “inf–sup” condition, and ensures the existence and uniqueness of the solution of the discretized Stokes equation (Bercovier and Pironneau, 1977). On the contrary, the P1–P1 element does not

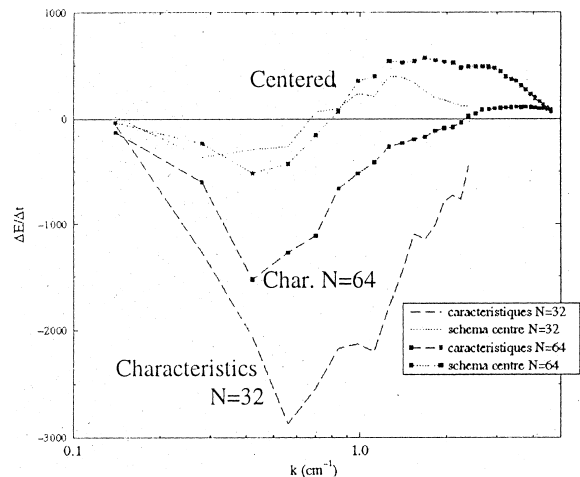


Fig. 1. Spectral transfer function $T(k)$ in grid turbulence.

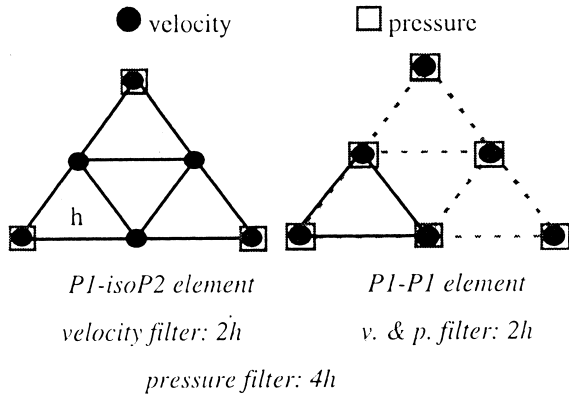


Fig. 2. Choice of elements (in 2D).

satisfy this condition and can provide spurious pressure modes.

The modes are damped out by penalty method (Girault and Raviart, 1986), i.e., a direct discretization of the Laplacian (called “non-compatible”) is blended with the (“compatible”) Laplacian resulting from the combination of “Divergence” and “Gradient” operators. The blending (or “Arakawa”) factor is always less than 5%. These modes appear mainly when the grid is generated by splitting an initially cartesian grid, but the correction is hardly necessary when the grid is fully unstructured.

Since the filter is implicit in the numerical scheme, it is clear that the filter-width for pressure is twice as that for velocity in the case of P1–isoP2 element (see Fig. 2). The interactions between resolved and subgrid-scales are thereby modified so it may be necessary to develop new subgrid-models. On the other hand, the filter-widths are identical for velocity and pressure for the P1–P1 element.

The treatment of incompressibility is also important. Brezzi and Fortin (1991) defined a constraint ratio: the ratio between numbers of pressure degrees of freedom and velocity degrees of freedom. In 3D, this ratio is equal to 1/3 for P1–P1 element and to 1/4 for P1–isoP2 element. Hence, the P1–isoP2 element is weakly compressible. Pelletier et al. (1989) emphasise one consequence of this behaviour

$$\| \mathbf{u} - \mathbf{v}_h \| \leq C \left\{ \underbrace{\inf_{w_h \in V_h} \| \mathbf{u} - w_h \|}_{\text{velocity}} + \underbrace{\inf_{q_h \in Q_h} \| p - q_h \|}_{\text{pressure}} \right\},$$

with \mathbf{u} and p the solutions of the continuous Stokes problem, \mathbf{v}_h and p_h the solutions of the discrete problem. The accuracy of the velocity depends both on the approximations of the velocity and pressure.

A laminar test-case highlights the effect of the low resolution of the pressure. In the “Taylor–Green” vortex flow, the shape of the cellular vortices remains unchanged. The analytical solution is known

$$U = -\sin(kx)\cos(ky)e^{-2vt}, \quad V = \cos(kx)\sin(ky)e^{-2vt},$$

$$P = \frac{1}{4}[\cos(2kx) + \cos(2ky)]e^{-4vt}.$$

The test is conducted with coarse resolution: eight points per waves for velocity. After 50 time steps, the L^2 error in the velocity component u is 0.08 for P1–P1 and 0.19 for P1–isoP2. Fig. 3 shows that the angles and vector amplitudes of velocity and pressure gradient are well captured by P1–P1 but not by

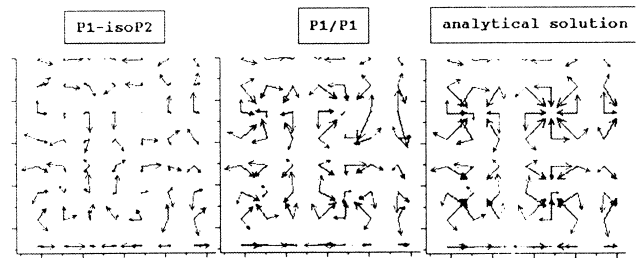
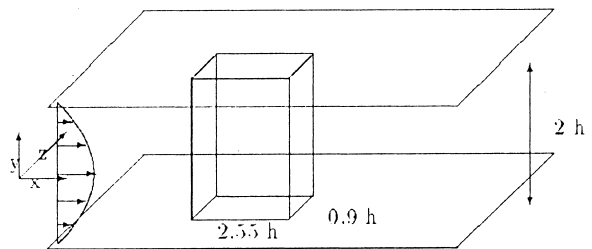


Fig. 3. Under-resolved Taylor vortices. Light grey: velocities. Dark grey: pressure gradients.

P1–isoP2. This is very important because the energy exchanges between velocity components are driven by the velocity–pressure gradient correlation, as can be seen from the RANS Reynolds Stress transport equations. The treatment of incompressibility (i.e. the pressure resolution) appears to be more important in this case than the satisfaction of the inf–sup condition.

2.3. Analysis of numerical choices in LES of channel flow

Channel flow computations are a common bench-mark for LES codes. The “minimal flow unit” was first introduced by Jimenez and Moin (1991): the computational box is large enough to sustain turbulence but contains only one or two wall structures (“streaks”). The streamwise, wall-normal and spanwise directions are, respectively, x , y and z .



The computational domain is $[2.55h, 2h, 0.9h]$, h being the half width of the channel. Periodicity is imposed in the x - and z -directions. The grid for our LES is composed by 157 925 nodes, deployed in 25 planes in the z -direction (Fig. 4).

The present LES results are compared to the DNS of Boudjemadi (1996). The Smagorinsky model ($C_s = 0.065$) with a Van Driest damping function was used. Since the ratio v_i/v is smaller than 10% everywhere, this is a quasi-DNS, i.e. a good test-case for the numerical method. Three numerical methods were tested:

- A: characteristics scheme and P1–isoP2 element.
- B: centred AB–CN scheme on P1–isoP2 element.
- C: centred on collocated P1–P1 element.

The spatial averaging is applied in planes parallel to the wall. Moreover, and since the computational box contains few structures, a long-time integration is also necessary to obtain reliable statistics. The time averaging was carried out over 330 time units (tU_0/h).

2.4. Time scheme advancement

Fig. 7 shows the time history of the maximum velocity. Scheme B captures high frequency oscillations, which are

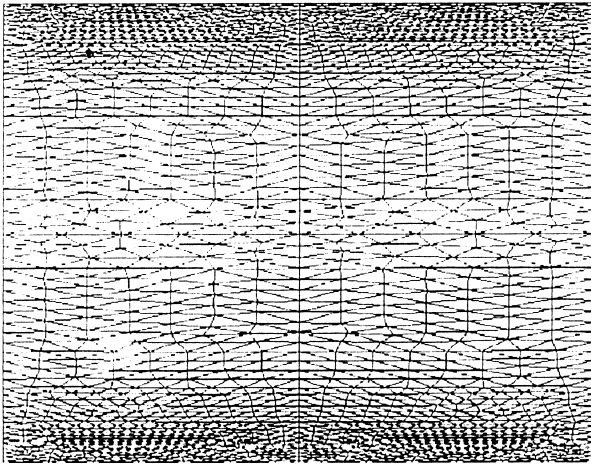


Fig. 4. Unstructured mesh in (x, y) plane for channel LES.

characteristics of turbulent flows, whereas scheme A provides a smooth evolution due to its low accuracy in time. The rms-values of the fluctuating velocities are shown in Fig. 5. The numerical viscosity of scheme A (characteristics) damps the normal fluctuations, which are severely underestimated. Schemes B (centred + P1–isoP2) and C (centred + collocated) seem equally satisfactory, the latter being somewhat superior in predicting the normal and spanwise fluctuations at the channel centre.

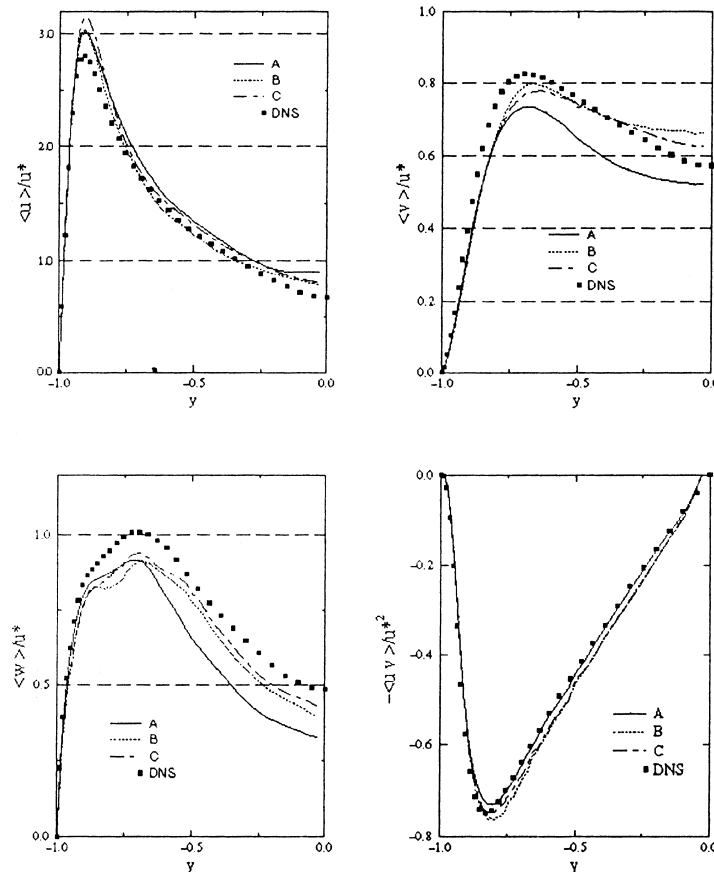


Fig. 5. RMS values for channel flow.

The snapshots of vorticity (not shown) and fluctuation isocontours (Fig. 6) reveal that scheme A gives excessively smooth structures near the wall. Since the normal fluctuations are underestimated, the turbulent structures do not migrate towards the centreline as well as in schemes B and C. Scheme A does not capture the essential features of this turbulent flow and will not be used in subsequent simulations. Reasons for choice of scheme C over of B are explained in the following section.

2.5. Driving pressure gradient

In LES of channel flow, it is often felt more natural to maintain a prescribed flowrate by adapting the mean pressure gradient at each time step, rather than re-scaling the instantaneous inlet velocities. The mass flux is here sustained by a mean pressure gradient F_1 . At each time step, F_1 is function of the variation of mass flux (Deschamps, 1988):

$$F_1^{n+1} = F_1^n + \rho \frac{(Q^n - Q_{ref}) - \frac{1}{2}(Q^{n-1} - Q_{ref})}{\Delta t L_z h}$$

with Q the flux, Q_{ref} the imposed flux and L_z the length of the computational box in the homogenous direction.

Fig. 7 shows the time history of this external force. For scheme A, a balance between pressure gradient and friction exists, and both are nearly constant. The centred scheme breaks up this equilibrium and allows larger mean pressure gradient fluctuations. By improving the pressure resolution, scheme C

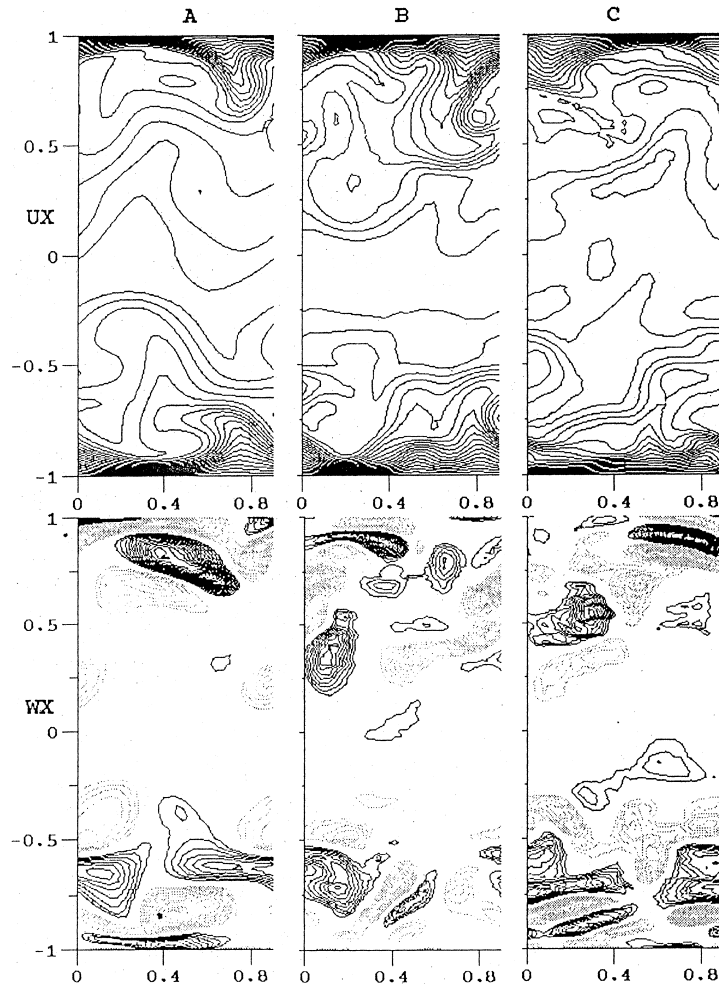


Fig. 6. Instantaneous streamwise and spanwise velocity contours in the (y, z) plane.

recovers this balance. As seen for the Taylor–Green vortex case, identical resolution of velocity and pressure catches the energy exchanges. For the minimal “flow unit”, the mean pressure gradient is linked to the mass flux: the poor behaviour of Scheme B is attributed to the weak mass conservativity of the P1–isoP2 element in the LES context.

In RANS models, the velocity–pressure gradient correlation drives the energy exchanges between velocity components. This term is evaluated from the instantaneous fields and is split into two parts:

$$\Pi_{11} = -\frac{1}{\rho} \left\langle \bar{u}' \frac{\partial \bar{p}'}{\partial x} \right\rangle - \frac{2}{\rho} \left\langle \bar{u}' F_1' \delta_{11} \right\rangle.$$

The perturbation induced by the forcing term $\langle \bar{u}' F_1' \rangle$ is compared to

$$\left\langle \bar{u}'^2 \right\rangle^{1/2} \left\langle F_1'^2 \right\rangle^{1/2}.$$

For Scheme B this term is of the same order as the mean resolved correlation. Thus the pressure gradient correction used to maintain the flowrate seems to introduce an unacceptable numerical artefact. For scheme C this ratio is less than 10%.

Finally, Fig. 8 shows the balance of the wall normal fluctuation equation. The \bar{u}'^2 budget is usually shown since the large production term masks defects in the other, smaller, terms. Complete resolution of the dissipation is not expected in LES, but the figure indicates that scheme A is particularly poor in this regard. This also shows on the imbalance. Underestimation of v' also affects the turbulent transport.

The final LES version (N3S-LES) is thus significantly different from the original code. It is based on a space-and-time-centred, collocated FEM scheme, with linear basis functions on tetrahedral elements.

To conclude, the surprising finding is that methods which are usually recommended in finite element textbooks, and have been successfully applied to RANS, are not suitable for LES.

3. Crossflow in tube bundle

The flow in a tube bundle is of great interest to the power generation industry, not only for the study of the performance of heat exchangers. Safety studies require predictions of vibrations caused by fluid–structure coupling or large temperature fluctuations that eventually lead to thermal stripping. The geometry is relatively simple, yet the flow experiences complex strains, making this an attractive test case.

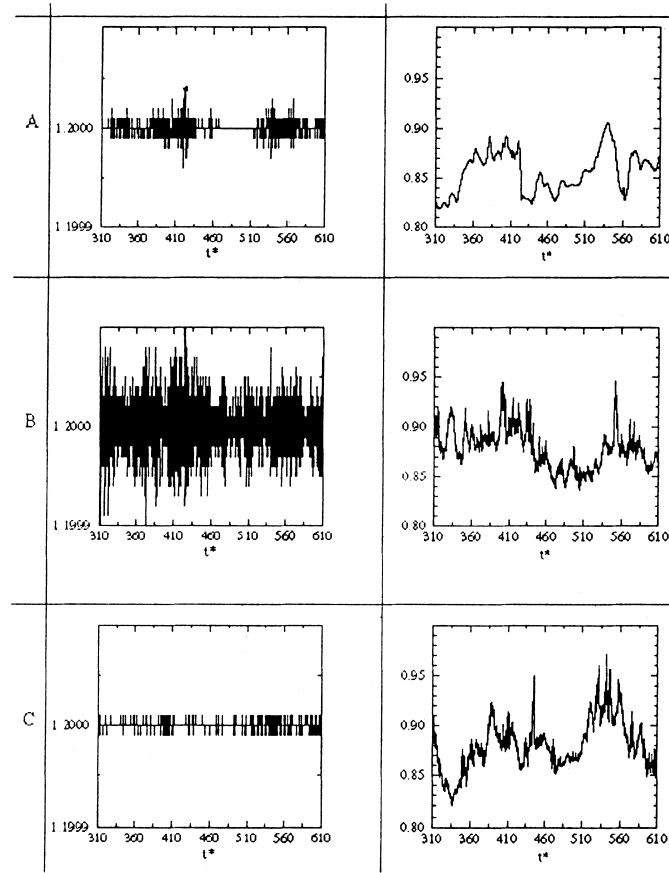


Fig. 7. Driving pressure gradient, F_1 (left), and maximum velocity (right) as function of time.

3.1. A challenge for RANS simulations

This flow was considered for the ERCOFTAC/IAHR Workshop on Turbulence Modelling held at UMIST, 15 and 16 June 1993. The experiment of Simonin and Barcouda (1988) provided data on mean velocities and Reynolds stresses for the flow through an staggered array of tubes (see Fig. 9). The tube diameters are $D = 21.7$ mm, and the distance between in-line cylinders is $L = 45$ mm. The Reynolds number based on the bulk velocity in the sub-channel in between the tubes, and the tube diameter is 40 000.

A variety of models (low Re $k-\epsilon$ models, Reynolds stress transport, both “standard” and “realisable” were applied (Appendix A). Some of the conclusions of that workshop, as presented by Hanjalic and Leschziner (1993) are the following:

- Velocity profiles are predicted generally reasonably well, but the stress profiles are poor, *particularly in the impinging region*.
- None of the results show indisputable superiority, though every model refinement and upgrade seems to make a positive contribution.
- *Disappointing*: Performances of RSM, though some improvements are discernible (stress behaviour in the impingement region).

The following workshop, Lisbon 94, again considered staggered tube bundles (Hanjalic and Hadzic, 1998). Additional experimental data from McGrath (1991) and Kelemenis (1993) were used, but the former provided only near wall data,

while some inconsistency with regard to mass conservation were found in the latter. Again performance of RANS models were disappointing while interestingly, results obtained with a lattice Boltzman scheme compared fairly well to the near wall data.

Sebag et al. (1991) devoted his thesis to the application of standard and elaborate second moment closures to this flow, and concluded that the major improvement in predicting the Reynolds stresses came from a quite simple correction to the dissipation equation (“sensitising dissipation to the anisotropy invariant” as proposed by Craft and Launder (1991)) and not from the modelling of the pressure strain term to cubic order. Meyer (1994), using his own experimental database which includes heat transfer, also pointed out at the limitations of second moment closures for tube bundle flow, attributing part of the difficulties to the very high turbulence intensities (35%).

3.2. LES computations

Finally, after the validation of N3S-LES, it seemed natural to consider again the experiment of Simonin and Barcouda (1988). The computational domain is sketched in Fig. 10. It is the minimum domain for the instantaneous field that does not impose artificial symmetries. The results will show that no coherent large structure (that might have been generated by imposing periodicity on a smaller domain) appears. A 2D mesh is generated, structured in the boundary layers, and free (Voronoi) far from the cylinders. Thirty-three identical planes

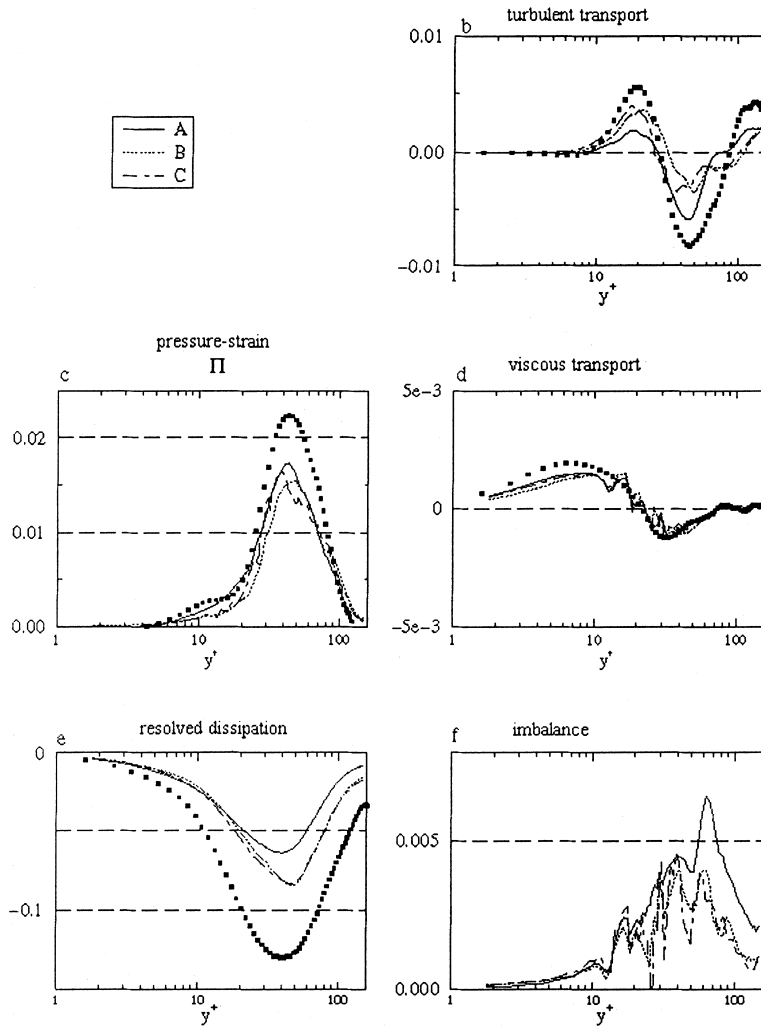


Fig. 8. Budget of the wall normal Reynolds stress.

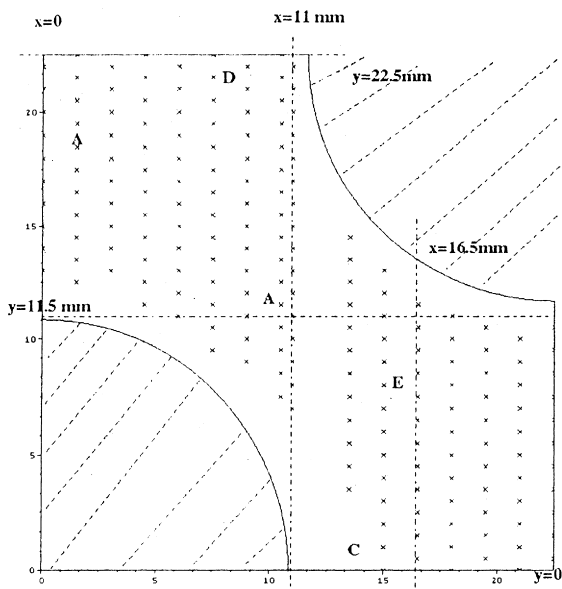


Fig. 9. Subchannel in the tube bundle experiment of Simonin and Barcouda (1988). Crosses indicate measurement locations.

are created in the z -direction, and the resulting prisms are cut into tetrahedra, producing a total of 405 312 nodes (see Fig. 11).

The Reynolds number in the LES computation based on bulk velocity in the narrowest section was set to 16 000. With a mean friction velocity of $u^* = 7 \text{ mm s}^{-1}$, the first grid point varies from $y^+ = 1.5$ to 4 wall units on the circumference of the cylinder. Because local instantaneous values

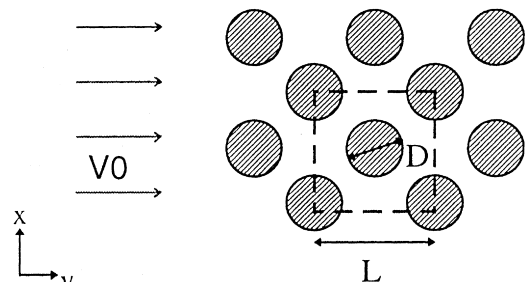


Fig. 10. Simonin and Barcouda (1988) experiment, computation sub-domain.

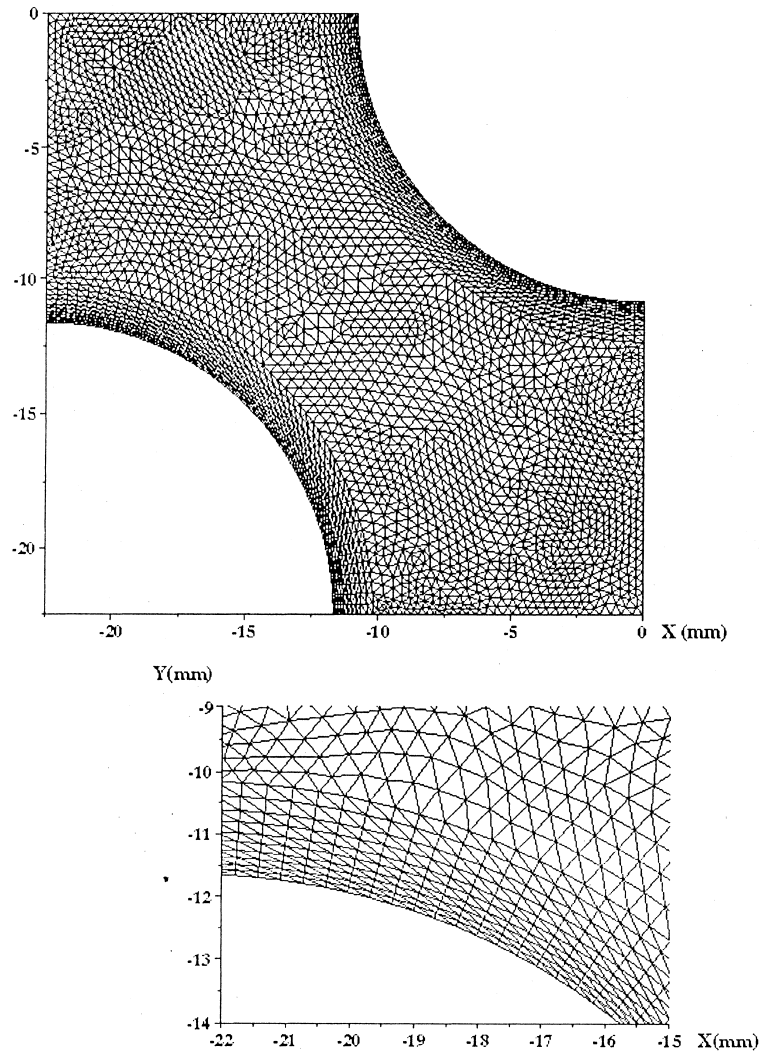


Fig. 11. Top: view of 1/4th of a 2D section of the mesh. Bottom: details of the near wall mesh.

can be significantly higher, wall functions are activated whenever needed, relating the wall stress value to the velocity at one cell height away from the wall (Werner and Wengle, 1991). The difference in the Reynolds number (16 000 instead of the 40 000 of the experiment) is expected to have little influence in this flow where the turbulent intensity is 35% (in contrast to flow around a single cylinder with laminar inflow).

A first run was computed with the Smagorinsky model (MS simulation), and after initialisation, statistics were accumulated over 1.745 s, i.e. three domain flow-through times; this was found sufficient since spanwise averaging and symmetries are used in gathering statistics. For the second run, with the localised dynamic procedure of Piomelli and Liu (1994), statistics were computed over five-domain flow-through times (3.468 s) (see Fig. 12).

The value of the Smagorinsky constant was set to $C_s = 0.065$, the dynamic model yielded somewhat higher average values of this coefficient, with great spatial variability, large values occur in the separated shear layers, and slightly negative values appear near the wall on the upstream half of the tube.

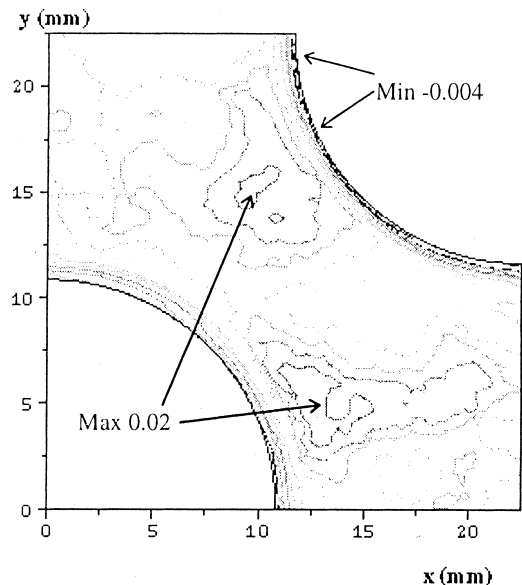


Fig. 12. Iso-contours of the SGS viscosity obtained with the dynamic model.

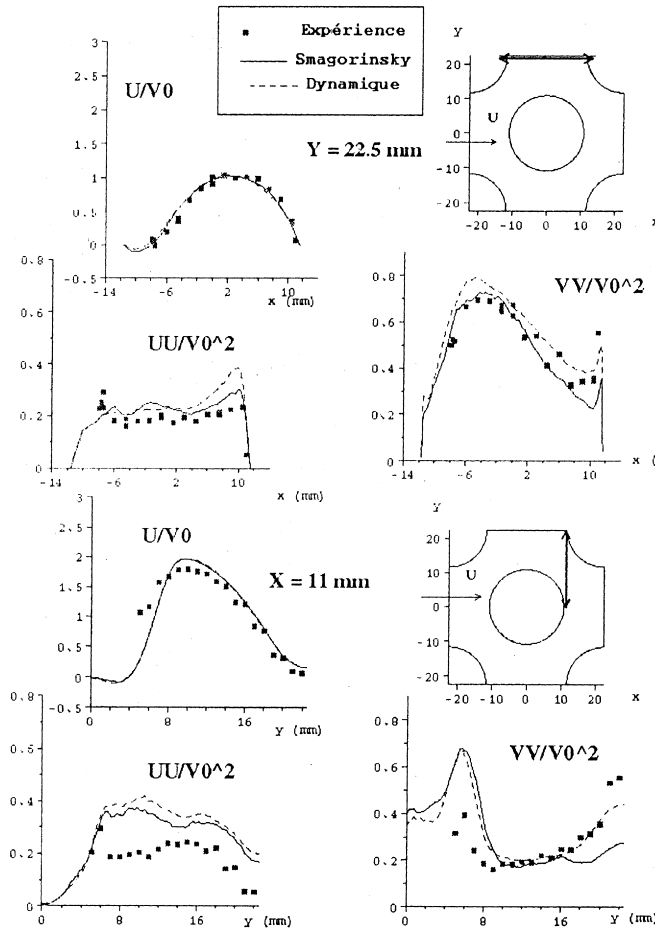


Fig. 13. First and second moments, solid lines: LES with Smagorinsky model, dashed lines: LES with dynamic model, symbols: experiment (see Fig. 9).

3.3. Statistical results

For the mean velocity, the agreement of the LES with all available data is excellent, and the results obtained from the two subgrid-scale models cannot be distinguished. For the Reynolds stresses, the overall agreement is fairly good. For sake of brevity, we will concentrate on two profiles where RANS models have the most difficulty. Fig. 13 shows the results on the wake to impingement axis and on the cross section just behind the tube. The striking and unusual feature observed on the wake axis is that the transverse velocity fluctuations are far larger than the axial ones. Thus as the flow approaches the stagnation point, $\overline{u^2} < \overline{v^2}$, and since $\partial\overline{U}/\partial x < 0$, the production of the stresses and kinetic energy are:

$$P_{uu} = -2\overline{u^2} \frac{\partial\overline{U}}{\partial x} > 0, \quad P_{vv} = +2\overline{v^2} \frac{\partial\overline{U}}{\partial x} < 0,$$

$$P_k = -(\overline{u^2} - \overline{v^2}) \frac{\partial\overline{U}}{\partial x} < 0.$$

We notice from the experiment and LES that $\overline{u^2}$ is fairly constant (production balances dissipation) in the impingement region while $\overline{v^2}$ decreases rapidly due to dissipation and negative production. Since $\overline{u^2} < \overline{v^2}$, the kinetic energy is also decreasing, in contrast to what is found at a stagnation point on

a single bluff body, or an impinging jet. Very near the stagnation point, the kinematic blockage by the wall forces u^2 fluctuations to be converted into v^2 (“wall echo effect”), and the dynamic model seems to better capture the peak in $\overline{v^2}$ better, although there is only one experimental point to suggest the existence of such a peak.

This sharp rise in $\overline{v^2}$ results in a sharp dip in P_k . Fig. 14 shows the dramatic overestimation of production by the second moment closure (note the different scaling). The experi-

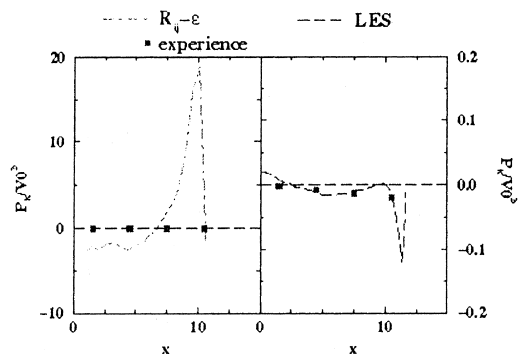


Fig. 14. Production on the stagnation point axis.

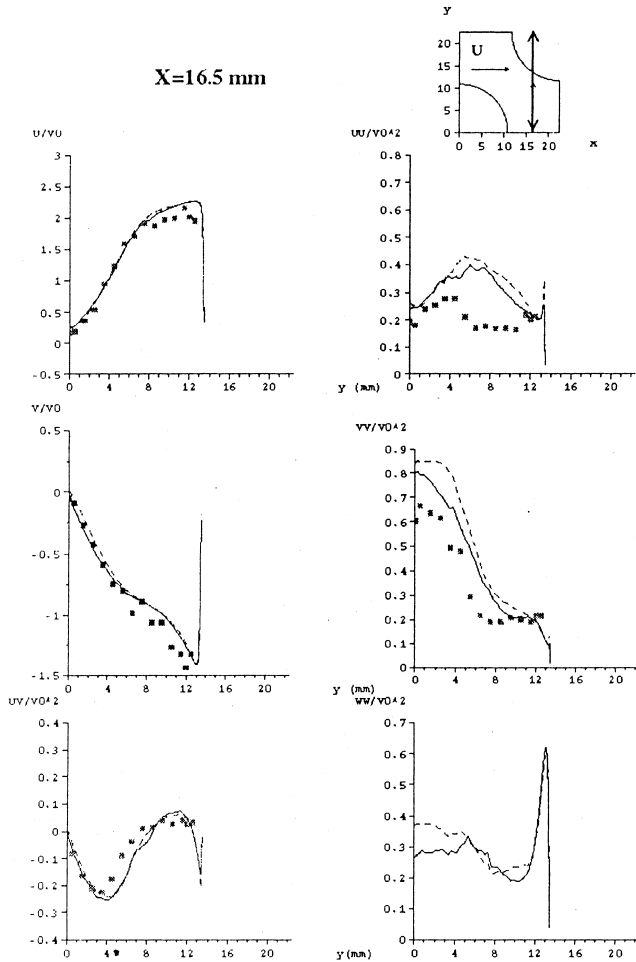


Fig. 15. See Fig. 13.

ment shows slightly negative values, but data are not available very close to the wall to confirm the sharp dip in P_k predicted by the LES.

In the cross section just after the tube (Fig. 13, bottom) at $X = 11$ mm, the first peak in $\overline{v^2}$ is due to the detached shear layer. The second peak corresponds to the stagnation point, and in this case there are a sufficient number of experimental points to confirm that the trend given by the dynamic model is more accurate than that produced by the Smagorinsky model. We noted earlier that the main difference between the Smagorinsky and dynamic models is that the latter predicts zero or negative eddy viscosity in the impingement region. This probably occurs because the high strain reduces spectral energy transfer. In turn, vanishing SGS dissipation allows the build up of $\overline{v^2}$. On the other hand, both models overestimate u^2 .

Further downstream, at $X = 16.5$ mm (Fig. 15) we again see excellent agreement with the experimental data for U and V components, including the extent of the recirculation bubble. Notice also the very large values of the w' fluctuations compared to u' and v' , near the upper cylinder, presumably due to the “wall echo” effect.

Overall, there is admittedly a systematic overestimation of $\overline{u^2}$ in the core region of the flow. Since the subgrid-scale viscosity is five times the molecular viscosity in most regions, limitations of the subgrid-scale modelling can be expected, but in any extent, discrepancies and subgrid-scale model

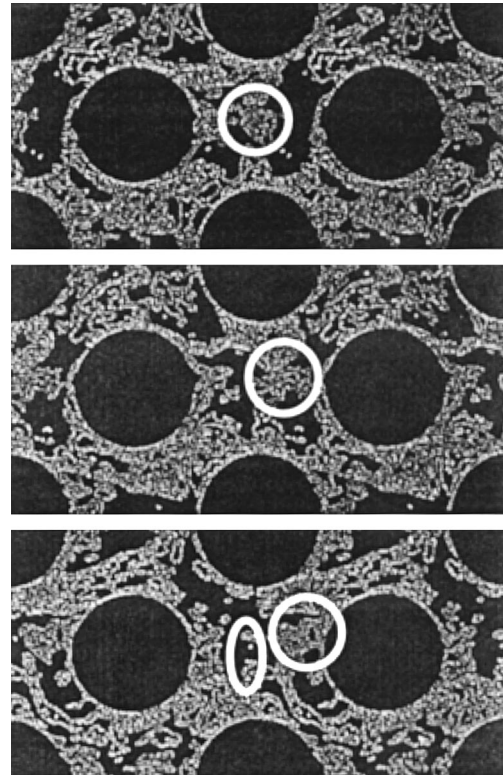


Fig. 16. Time sequence of instantaneous iso-streamwise velocities.

dependencies are much smaller than the extreme variability observed in the aforementioned workshops on RANS models.

3.4. Instantaneous velocity fields

Visualisations of the instantaneous streamwise velocities (Fig. 16) show that large regions of low velocity (in light grey,

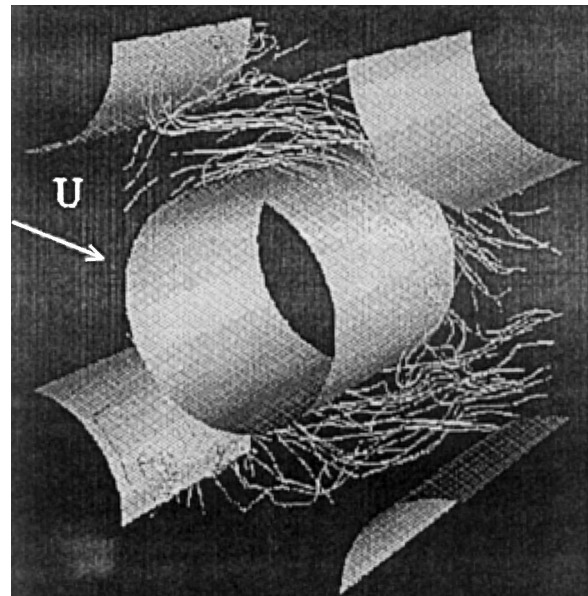


Fig. 17. Particle lines emitted from a vertical line.

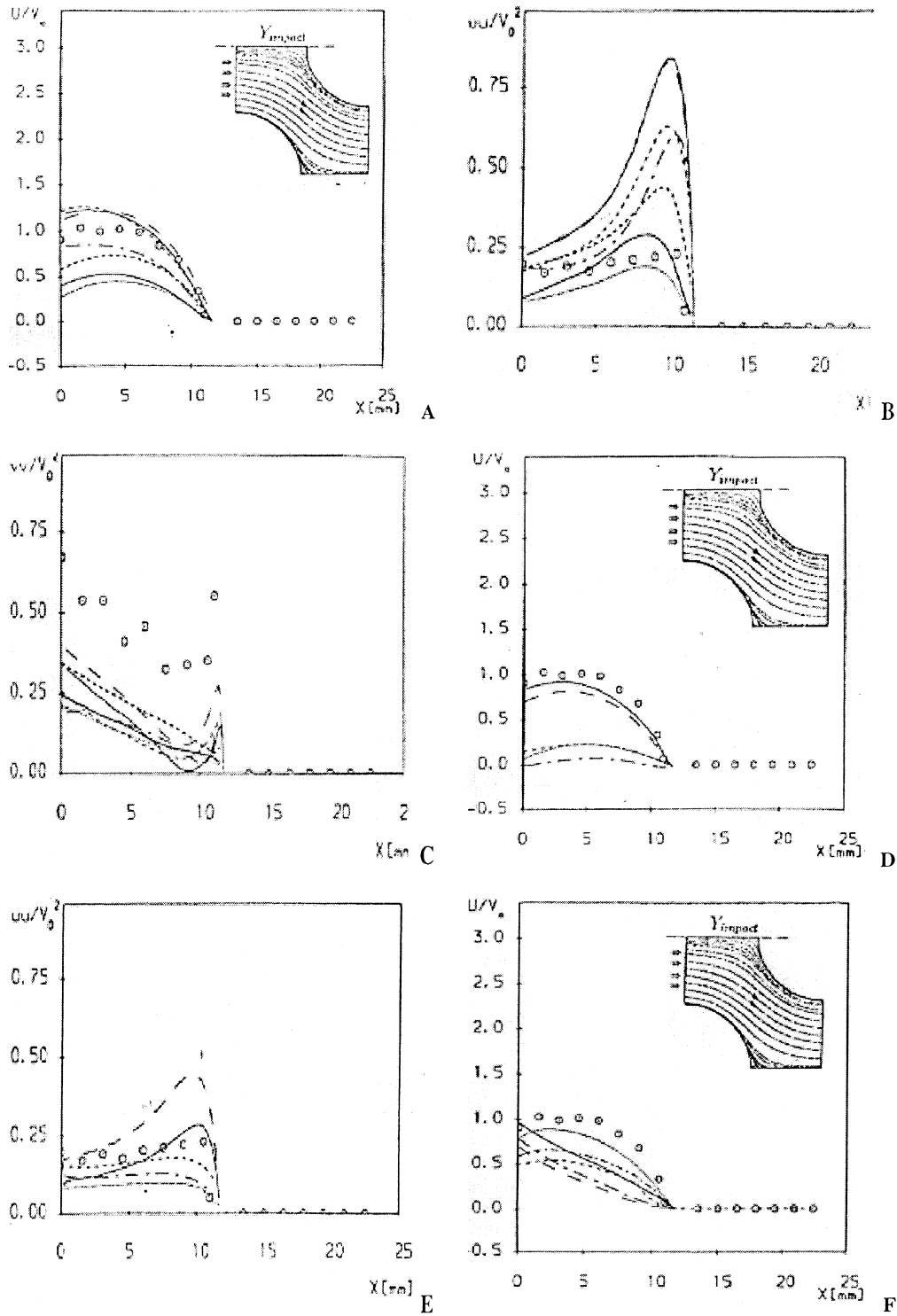


Fig. 18. (A),(B),(C) Various low Re two-equation models. The three sets of data (UMIST) corresponding best to the exp; for the mean velocity (A) correspondingly given the highest turbulent kinetic energy levels. (D), (E) RNG models. Models were checked to be identical, the large differences observed are attributed to a bifurcation: as the kinetic energy level is reduced by the RNG correction, the flow is allowed to stagnate in between tubes, with little mixing from the principal flow passing the tubes with a minimum meandering effect. Less mean flow deformation in turn yields less turbulence production. (F), (G), (H) Second moment closures standard IP model seems to yield the “best” results yet $\overline{v^2}$ is severely underestimated. (I), (J) Cross-section after the tube (cf. Fig. 15).

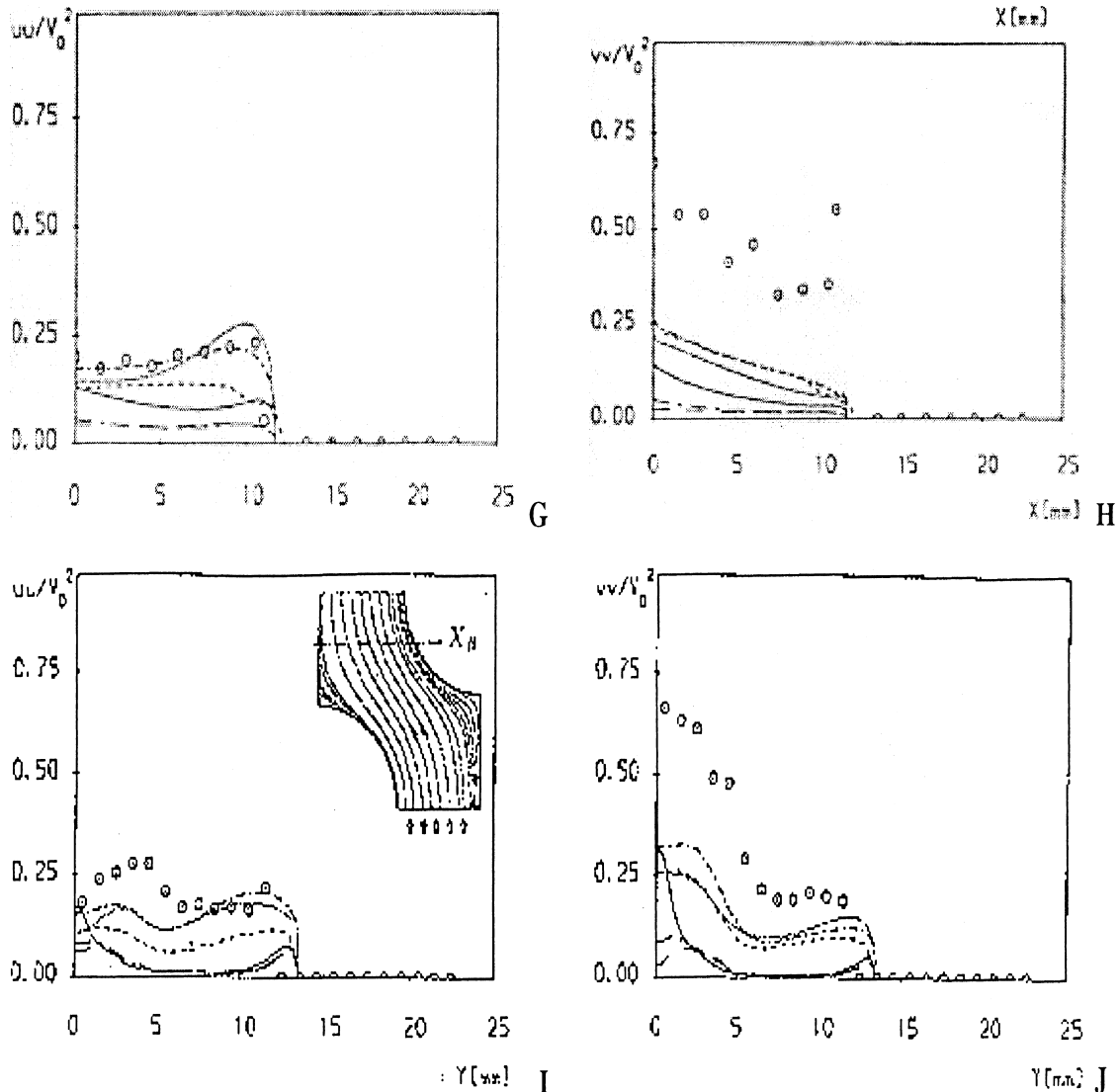


Fig. 18. (Continued)

in circle) are detached from the cylinder into the wake and transported towards the stagnation point (flow is from left to right). High velocity blobs (dark grey, in ellipse) make occasional incursions in this region. An explanation of the difficulties encountered by standard RANS models may be that in this wake-to stagnation gap region, the fluctuating velocities are larger than the mean. It is thus difficult to reconstruct the flow characteristics just from the mean velocity. In particular, the so-called “wall echo effect” introduced in second moment closures were devised to represent the “splating” of small eddies against an infinite (compared to the integral scale) plane wall. In the present case, as seen from the instantaneous fields, the size of the structures is comparable to the cylinder radius. These eddies are large enough to be affected by the curvature of the wall. At the stagnation point one can imagine that the wall normal fluctuations are transferred into lateral fluctuations more easily because of this strong curvature.

Finally, we have pointed out the relatively large velocity fluctuations in the homogeneity direction. This is illustrated in Fig. 17. Particles emitted from a vertical line, normal to the

tube axis, are spread out in the whole spanwise dimension, showing the highly 3D nature of the flow. This flow is probably an ideal case for the modelling the mysterious “wall echo” terms. Indeed they play here a dominant role, since overall, the w' fluctuations (for which there is no direct production) are significantly larger than the streamwise fluctuations which are alternatively generated by shear and damped by cinematic blocking.

4. Conclusions and perspectives

It has been shown that a standard “industrial” finite element code cannot be straightforwardly used for LES which requires specific discretizations. The low-order FE scheme was tested on turbulent flows. This analysis underlines that the “safest” element is not well adapted to LES.

We stress here that for the grid turbulence and channel flow simulations, the point was not to produce a database, but to exhibit the problems that arise while using a numerical

scheme for unstructured grids (and aiming at complex geometries). For instance, correct grid turbulence spectra can be produced with an upwind scheme thanks (but by chance) to the fact that the dynamic model can compensate numerical diffusion by decreasing the eddy viscosity. But dramatic resolution sensitivity was exhibited on the (rarely shown) energy transfer function. For channel flow, the wall normal stress budget is shown, instead of the (more popular) streamwise stress exhibiting more flattering comparisons thanks to the large production term (related to the larger, easily captured eddies). Scarce honest presentations of low order schemes applied to LES are found in the literature, with the notable exception of Kravchenko and Moin (1997) where similar underestimations of the wall normal fluctuations are exhibited for second-order schemes (see Fig. 11), these authors advocating higher order schemes. From several but private communications, channel flow simulation using structured grids and collocated schemes produce significantly damped results compared to staggered arrangements using similar resolutions. We stress here that in addition to the order of the scheme, the variable arrangement is highly important in LES, where eddies need to be captured on only a couple of cells, the staggered arrangement seemingly having unique properties, but not easily extended to unstructured grids.

The LES simulation of the flow in a tube bundle yielded excellent agreement with experimental data, whereas previous RANS simulations had failed. This is not “beginner’s luck”, LES was successful because the size of the larger eddies are similar to those of the obstacles. RANS models encounter limitations when the integral length-scale of the turbulence is comparable with that of the mean flow inhomogeneity (this interpretation was proposed concerning the effect of the Reynolds number on the recirculation behind a step (Laurence and Parneix, 1997)). Thus it seems that to much effort has been devoted to simple flows, e.g. channel flows, where RANS models yield excellent results with much less computational effort. LES and RANS should not be considered to be in competition. LES of the boundary layer on airfoil at low incidence will remain out of reach for very long time, given the small size of the turbulent structures compared to the airfoil, while RANS models may be sufficient for such flows (without separation). On the other hand small bluff bodies, e.g. electronic components in a highly turbulent channel flow, as considered in the 1997 ERCOF-TAC/AIHR workshop seems an application in which LES is preferable.

As concerns subgrid scale models, overall, the “dynamic model” was not proved to produce superior results compared to the Smagorinsky model, except at the stagnation points of the tube bundle. However, the “dynamic model” does not require preliminary tuning for the specific nature of the code or flow, and is thus believed “safer” for an overcost of less than 5%.

A logical follow-on of the present simulation is heat transfer, but a new project, in collaboration with the French atomic energy commission (CEA), has started with the objective of developing an LES code for unstructured meshes for massively parallel computers (T3E). The aim is to perform LES of complex geometries with over 10 million nodes, and the tube bundle test case is being considered again (on a larger domain), hopefully providing complete data including heat transfer. A finite volume unstructured and staggered-like arrangement is also attempted, and seems promising compared to the present collocated scheme.

Appendix A. RANSE 1993 Workshop Results (15) (all graphs by T. Craft)

See Fig. 18.

References

- Bercovier, M., Pironneau, O.A., 1977. Error estimates for finite element method solution of the Stokes problem in the primitive variables. *Numer. Math.* 33, 211–224.
- Boudjemadi, R., 1996. Simulation numérique directe et modélisation de la convection naturelle turbulente dans un canal différentiellement chauffé. PhD thesis, Paris VI.
- Brezzi, F., Fortin, M., 1991. *Mixed and Hybrid Finite Elements*. Springer, Berlin.
- Chabard, J-P., Métivet, B. et al., 1992. An efficient finite element method for the computation of 3D turbulent incompressible flows. *Finite Elements in Fluids*, vol. 8.
- Craft, T.J., Launder, B.E., 1991. Computation of impinging flows using second-moment closures. *Turbulent Shear Flows 8*, Technical University of Munich.
- Deschamps, V., 1988. Simulation numérique de la turbulence inhomogène incompressible dans un écoulement de canal plan. PhD thesis, INPT.
- Ducros, F., Nicoud, F., Shonfeld, T., 1997. LES of compressible flows on hybrid meshes. *Turbulent Shear Flow 11*. Grenoble, France.
- Girault, V., Raviart, P.A., 1986. *Finite Element methods for Navier–Stokes equations. Theory and Applications*. Springer, Berlin.
- Hanjalic, K., Hadzic, I., 1998. Third ERCOF-TAC/IAJR Workshop on Refined Flow Modelling. T.U. Delft, Applied Physics.
- Hanjalic, K., Leschziner, M., 1993. Report-back on ERCOF-TAC/IAHR Turbulence Modelling. Workshop held at UMIST, 15–16 June.
- Horiuti, K., 1987. Comparison of conservative and rotational forms in LES of turbulent channel flows. *J. Comput. Phys.* 71, 343–370.
- Jansen, K., 1993. Unstructured grid large eddy simulation of wall bounded flow. *Ann. Res. Briefs CTR*, Stanford.
- Jimenez, J., Moin, P., 1991. The minimal flow unit in near-wall turbulence. *JFM* 225, 213–240.
- Kelemenis, I., 1993. PhD thesis. University of Manchester.
- Kravchenko, A.G., Moin, P., 1997. On the effect of numerical errors in large eddy simulations of turbulent flows. *J. Comput. Phys.* 131, 310–322.
- Laurence, D., 1985. Advective formulation of LES. In: Schuman, Friedrich (Eds.), *Direct and Large Eddy Simulation of Turbulence*, EUROMECH col. N 199. Munich.
- Laurence, D., Parneix, S., 1997. Second moment closure analysis of a DNS backstep flow database. In: *Turbulent Heat and Mass Transfer 2*. Delft University Press, Delft.
- McGrath, G., 1991. PhD thesis. Queen Mary and Weston College.
- Meyer, K.E., 1994. Experimental and numerical investigation of turbulent flow and heat transfer in staggered tube bundles. PhD thesis. AFM 94-03, Tech. Univ. of Denmark.
- Pelletier, D., Fortin, A.A., Camarero, R., 1989. Are FEM solutions of incompressible flows really incompressible? *Int. J. Numer. Meth. Fluids* 9, 99–112.
- Piomelli, U., Liu, J., 1994. Large eddy simulation of rotating channel flows using a localised dynamic model. *Phys Fluids A7*.
- Rodi, W., Ferziger, J.H., Breuer, M., Pourquié, M., 1997. Status of large eddy simulation: results of a workshop. *Journal of Fluids Engineering*.
- Rollet-Miet, P., 1997. Simulation des Grandes Echelles sur maillages non structurés pour géométries complexes. PhD thesis. Ecole Centrale de Lyon.
- Sebag, S., Maupu, V., Laurence, D., 1991. Non-orthogonal calculation procedures using second moment closure. *TSF* 8, 1991.

Simonin, O., Barcouda, M., 1988. Measurements and prediction of turbulent flow entering a staggered tube bundle. Fourth International Symposium on Applications of Laser Anemometry to Fluid Mechanics. Lisbon, Portugal.

Werner, H., Wengle, H., 1991. LES of turbulent flow over and around a cube in a plane channel. *Turbulent Shear Flows 8*, University of Munich.